Ihh controls cartilage development by antagonizing Gli3, but requires additional effectors to regulate osteoblast and vascular development

Matthew J. Hilton[1], Xiaolin Tu[1], Julie Cook[1], Hongliang Hu[1] and Fanxin Long[1,2,*]

[1]Department of Medicine, Washington University Medical School, St Louis, MO 63110, USA
[2]Department of Molecular Biology and Pharmacology, Washington University Medical School, St Louis, MO 63110, USA
*Author for correspondence (e-mail: flong@wustl.edu)

Accepted 1 August 2005

Development 132, 4339-4351
Published by The Company of Biologists 2005
doi:10.1242/dev.02025

Summary

Indian hedgehog (Ihh) controls multiple aspects of endochondral skeletal development, including proliferation and maturation of chondrocytes, osteoblast development and cartilage vascularization. Although it is known that Gli transcription factors are key effectors of hedgehog signaling, it has not been established which Gli protein mediates Ihh activity in skeletal development. Here, we show that removal of *Gli3* in *Ihh*-null mouse embryos restored normal proliferation and maturation of chondrocytes, but only partially rescued the defects in osteoblast development and cartilage vascularization. Remarkably, in both $Ihh^{-/-}$ and $Ihh^{-/-}$; $Gli3^{-/-}$ embryos, vascularization promoted osteoblast development in perichondrial progenitor cells. Our results not only establish Gli3 as a critical effector for Ihh activity in the developing skeleton, but also identify an osteogenic role for a vasculature-derived signal, which integrates with Ihh and Wnt signals to determine the osteoblast versus chondrocyte fate in the mesenchymal progenitors.

Key words: Ihh, Gli3, PTHrP (Pthlh), Wnt, β-Catenin, Cartilage, Bone, Vascularization, Mouse

Introduction

Indian hedgehog (Ihh) signaling is indispensable for proper development of the endochondral skeleton. In the developing cartilage, *Ihh* is primarily expressed by prehypertrophic chondrocytes (chondrocytes immediately prior to hypertrophy) as well as in early hypertrophic chondrocytes, and Ihh signals to both immature chondrocytes and the overlying perichondrial cells (St-Jacques et al., 1999; Vortkamp et al., 1996). $Ihh^{-/-}$ mice exhibited multiple defects in development of the endochondral skeleton, these including a 50% reduction in chondrocyte proliferation, profound dysregulation of chondrocyte maturation, a severe delay in cartilage vascularization and a complete lack of osteoblasts (Long et al., 2001; St-Jacques et al., 1999). Subsequent genetic analyses of smoothened (*Smo*), which encodes a seven-pass transmembrane protein indispensable for all Hh signaling, revealed that direct Ihh input was required for proper proliferation of chondrocytes and development of the osteoblast lineage (Long et al., 2004; Long et al., 2001). Regulation of chondrocyte maturation, however, did not require direct Ihh signaling in chondrocytes as it appeared to be mediated primarily via a secondary signal parathyroid hormone-related peptide (Pthlh) whose expression was dependent upon Ihh signaling (Karp et al., 2000; Long et al., 2001; St-Jacques et al., 1999). Regulation of cartilage vascularization by Ihh is less well understood. Mouse embryos with *Smo* conditionally removed by *Col2-Cre* exhibit normal vascularization (Long et al., 2001), indicating that Ihh controls vascularization independent of its signaling in chondrocytes. In chimeric embryos developed from wild-type and $Smo^{-/-}$ ES cells, $Smo^{-/-}$ cells contribute to the endothelium of blood vessels in the bone marrow cavity (Long et al., 2004), arguing against a requirement for direct Ihh signaling in endothelial cells for cartilage vascularization.

The role of vascularization in osteoblast formation during endochondral skeletal development is not well understood. Cartilage anlagen that prefigure the long bones are initially avascular; nascent vascularization coincides with osteoblast differentiation in the perichondrium. $Ihh^{-/-}$ mice exhibited profound defects in cartilage vascularization, and thus have not been informative in previous analyses for assessing the role of vascularization in osteoblast development in the endochondral skeleton. However, the skull bones did form in the $Ihh^{-/-}$ embryo (St-Jacques et al., 1999), indicating the presence of an Ihh-independent osteogenic pathway in the intramembranous bones.

Hh signaling is mediated through transcriptional regulation by the zinc-finger transcription factors Gli1, Gli2 and Gli3 in mammals, or Cubitus interruptus (Ci) in *Drosophila*. Mutant studies in the mouse demonstrated crucial roles for Gli2 and Gli3 in the developing embryo, whereas Gli1 appeared to be dispensable (Bai et al., 2002; Ding et al., 1998; Matise et al., 1998; Mo et al., 1997; Motoyama et al., 1998; Park et al., 2000), although additional phenotypes were noted when *Gli1* was deleted in the $Gli2^{-/-}$ background (Park et al., 2000). In particular, Gli2 appeared to function in vivo predominantly as

a transcriptional activator both in the central nervous system (Ding et al., 1998; Komori et al., 1997; Matise et al., 1998; Sasaki et al., 1999) and in the developing hair follicle (Mill et al., 2003). Gli3, however, was shown to function primarily as a transcription repressor of Hh targets. Removal of both *Gli3* and *Shh* in the mouse rescued a multitude of defects in specification of the ventral neuron types, patterning of the limb and lung organogenesis caused by the loss of *Shh* alone (Li et al., 2004; Litingtung and Chiang, 2000; Litingtung et al., 2002). However, additional studies have also revealed an activator function for Gli3 in both the somite and the spinal cord (Bai et al., 2004; Buttitta et al., 2003), and a repressor activity for Gli2 in the somite (Buttitta et al., 2003). These studies underline the diverse roles of the Gli molecules in mediating Hh signaling in different physiological contexts.

To determine the potential roles of Gli3 in mediating Ihh signaling during skeletal development, we have generated double mutant embryos of $Ihh^{-/-}; Gli3^{-/-}$, and have analyzed the skeletal phenotype. The results demonstrate that derepression of Gli3 accounts for multiple, but not all, aspects of Ihh signaling in the endochondral skeleton.

Materials and methods

Mouse strains

The $Ihh^{+/-}$ and $Gli3^{Xt\text{-}J}$ mouse strains are as previously described (Maynard et al., 2002; St-Jacques et al., 1999). The $Gli3^{Xt\text{-}J}$ strain was acquired through the Jackson Laboratory (Bar Harbor, Maine). The wild-type and deletion alleles of *Gli3* were detected by PCR as previously described (Maynard et al., 2002). Embryos of *Dermo1-Cre;* β-catenin$^{c/c}$ were generated as previously described (Hu et al., 2005).

Analyses of mouse embryos

Whole-mount skeletal staining of embryos was based on McLeod (McLeod, 1980). For analyses on sections, embryonic tissues were collected in PBS, fixed in 10% formalin overnight at room temperature, then processed and embedded in paraffin prior to sectioning at 6 μm. For detection of mineralization, sections were stained with 1% silver nitrate (von Kossa method) and counterstained with Methyl Green. For histology or in situ hybridization on E17.5 and E18.5 embryos, limbs were decalcified in 14% EDTA in PBS (pH 7.4) for 48 hours after fixation and prior to processing. In situ hybridization was performed as described previously by using ^{35}S-labeled riboprobes (Long et al., 2001). All in situ probes were as previously described (Hu et al., 2005; Long et al., 2004; Long et al., 2001), with the exception that the *Pthlh* probe was derived from a full-length cDNA clone (ATCC, catalog no. 7061403). For BrdU analysis, pregnant females were injected with BrdU at 0.1 mg/g body weight at 2 hours prior to harvest. Embryos were collected in ice-cold PBS, processed and sectioned as above. BrdU detection was performed using a kit from Zymed Laboratories (South San Francisco, CA) as per instructions. Labeling index was scored for a least four sections from various planes of section through the cartilage. Multiple wild-type and mutant pairs of littermates were analyzed and results from a representative pair are reported here.

Western analyses

For western analyses of Gli3, whole-cell lysates were prepared using a RIPA buffer [20 mM Tris (pH 8.0), 1% NP-40, 0.25% sodium deoxycholate, 150 mM NaCl, 0.1% SDS, 1 mM EGTA, 1 mM EDTA, protease inhibitor cocktail (Roche), phosphatase inhibitor cocktails 1 and 2 (Sigma, St Louis, MO)] from the fore- and hindlimb cartilage elements of E14.5 embryos. Cartilage was pulverized in liquid nitrogen using a mini-pestle (Clontech) prior to protein extraction. Total cell lysate (100 μg) was separated on a SDS-PAGE gel and a specific antibody (Li et al., 2004) was used to detect Gli3 by the ECL method (Amersham Biosciences). An antibody against α-catenin (Santa Cruz Biotechnology) was used as a loading control.

Results

A partial rescue of linear growth of endochondral bones in DKO embryos

We generated double mutant embryos of $Ihh^{-/-}; Gli3^{-/-}$ (DKO) by mating double heterozygous ($Ihh^{+/-}; Gli3^{+/-}$) mice. The $Gli3^{+/-}$ strain obtained from the Jackson Laboratory ($Gli3^{Xt\text{-}J}$) contains a deletion of 51.5 kb at the *Gli3* allele, which results in a non-functional fusion transcript that lacks the coding sequence for the DNA binding motif (Buscher et al., 1998; Maynard et al., 2002). Of 358 total embryos harvested between E13.5 and E18.5, 11 embryos were identified as DKO (3%). The reasons for the low recovery rate (expected Mendelian rate 6%) were not further investigated. The DKO embryos that developed to term all died at birth.

Whole-mount skeletal preparations from E18.5 embryos revealed that most skeletal elements of the DKO embryos exhibited an intermediate length between wild-type and $Ihh^{-/-}$ littermates (Fig. 1). This was most evident with the forelimb skeleton whose overall length was markedly increased in the DKO (Fig. 1A3) over the $Ihh^{-/-}$ embryo (Fig. 1A5), although the hindlimb skeleton showed a more modest increase in length (Fig. 1, compare B3 with B5). Notably, both limb skeletons of DKO embryos remained considerably smaller than those of either the wild-type (Fig. 1A1,B1) or the $Gli3^{-/-}$ embryos (Fig. 1A2,B2). The increase over $Ihh^{-/-}$ mutants in overall size of the skeleton was not evident in embryos of $Ihh^{-/-}; Gli3^{+/-}$ ($I^{-/-}; G^{+/-}$) in which one copy of *Gli3* remained intact (Fig. 1, compare A4 with A5, B4 with B5). In addition to a slight reduction in the length of long bones (Fig. 1, compare A1 with A2, B1 with B2), the $Gli3^{-/-}$ embryos exhibited a number of characteristic patterning defects in the limbs, including the absence of the deltoid tuberosity (Fig. 1A1, asterisk) in the humerus and a varying degree of truncation of the distal tibia (Fig. 1B2, big arrowhead). In addition, the $Gli3^{-/-}$ embryos invariably exhibited bifurcation of phalange 1 (P1) of all digits (Fig. 1B2, small arrowhead, out of plane of focus in A2) as well as polydactyly in both the forelimb (Fig. 1A2, digits 1-7) and the hindlimb (Fig. 1B2, digits 1-6, 2* representing syndactyly at digit 2). Importantly, all defects characteristic of the $Gli3^{-/-}$ embryo were maintained in the DKO embryo, including polydactyly, bifurcation of P1 (Fig. 1A3,B3, small arrowheads) and truncation of the tibia (Fig. 1B3, big arrowhead). These results indicate that Gli3 functions antagonistically with and genetically downstream of Ihh to regulate linear growth of the long bones.

Examination of the whole-mount stained skeletons at E18.5 also revealed that the bone collar was absent in most long bones of the DKO embryo. As in the $Ihh^{-/-}$ mutant (Fig. 1A5,B5), the metacarpal (‘mc’), metatarsal (‘mt’) and phalanges (‘p’) of the DKO embryo exhibited little or no mineralization (Fig. 1A3,B3). Also similar to those in the $Ihh^{-/-}$ mutant (Fig. 1A5,B5), the radius (‘r’) (Fig. 1A3) as well as the fibula (‘fi’) (Fig. 1B3) contained mineralized cartilage (stained dark red) but no bone collar. Interestingly, the ulna and the more

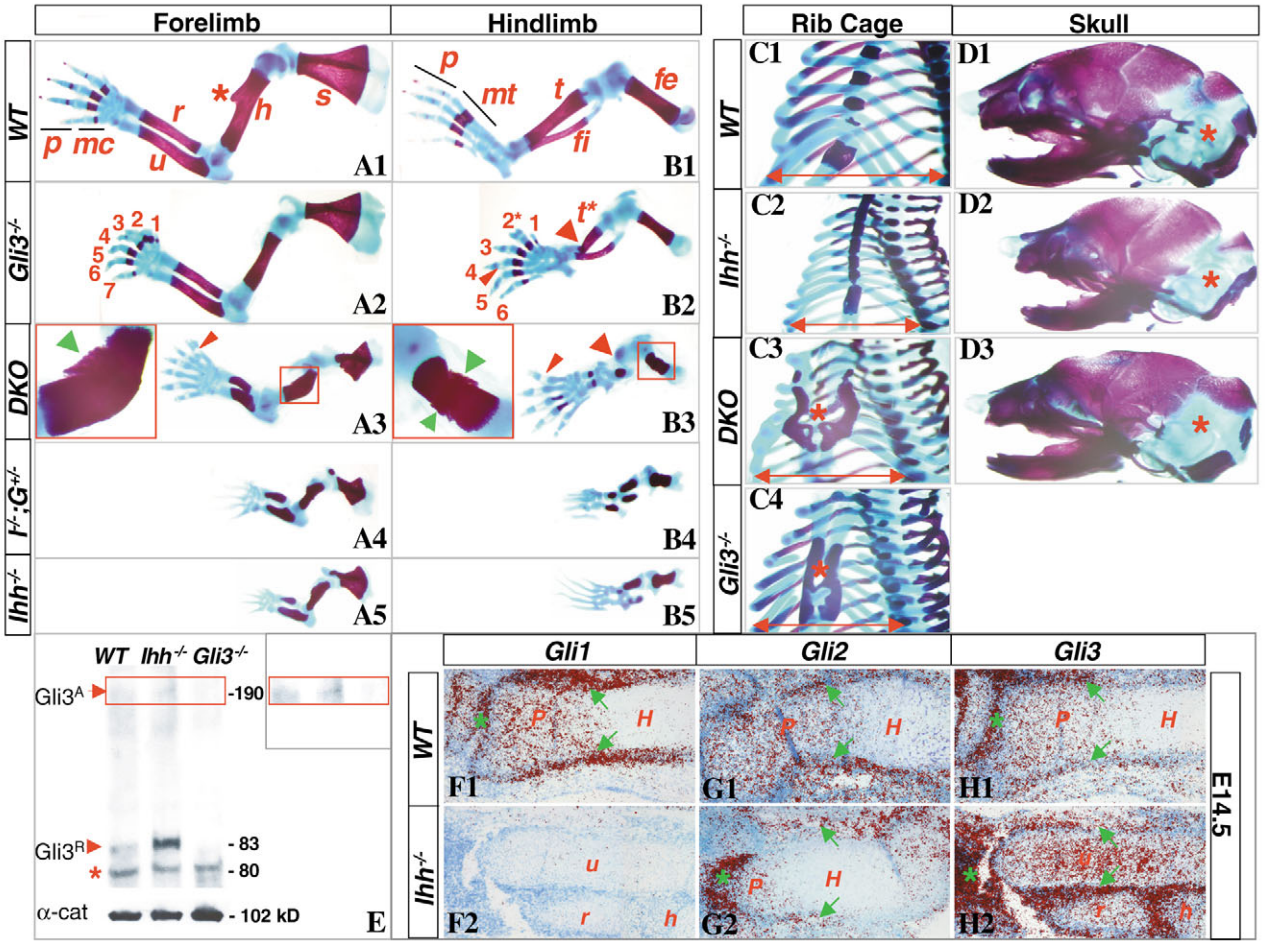

Fig. 1. Partial rescue of the skeletal growth in the DKO embryo at E18.5. (A1-A5) Forelimbs of embryos of various genotypes: wild type (A1), *Gli3*$^{-/-}$ (A2), DKO (A3), *Ihh*$^{-/-}$; *Gli3*$^{+/-}$ (*I*$^{-/-}$; *G*$^{+/-}$, A4) and *Ihh*$^{-/-}$ (A5). (A1) s, scapula; h, humerus; r, radius; u, ulna; mc, metacarpal; p, phalanges; *, deltoid tuberosity. (A2) Numbers 1-7 indicates polydactyly. (A3) Red arrowhead denotes bifurcation of the proximal phalange (P1). Inset shows higher magnification of boxed region. Green arrowhead indicates ectopic bone. (B1-B5) Hindlimbs from embryos of various genotypes: wild type (B1), *Gli3*$^{-/-}$ (B2), DKO (B3), *Ihh*$^{-/-}$; *Gli3*$^{+/-}$ (*I*$^{-/-}$; *G*$^{+/-}$, B4) and *Ihh*$^{-/-}$ (A5). (B1) fe, femur; t, tibia; fi, fibula; mt, metatarsal; p, phalanges. (B2) Numbers 1-6 indicates polydactyly. (B2,B3) Big red arrowheads indicate truncation of the tibia (t*). Small red arrowhead indicates bifurcation of the proximal phalange (P1). Inset shows higher magnification of boxed region. Green arrowhead indicates ectopic bone. (C1-C4) Rib cages from embryos of various genotypes: wild type (C1), *Ihh*$^{-/-}$ (C2), DKO (C3) and *Gli3*$^{-/-}$ (C4). Double-headed arrows (C1-C4) indicate the width of the rib cage. Asterisks (C3,C4) indicate the split sternum. (D1-D3) Skulls of embryos of various genotypes: wild type (D1), *Ihh*$^{-/-}$ (D2) and DKO (D3). Asterisks (D1-D3) denote the chondrocranium. (E) Detection of Gli3 in limb cartilage proteins. Gli3^{A}, the full-length (190 kDa) activator form of Gli3; Gli3^{R}, the truncated (83 kDa) repressor form of Gli3. α-cat., α-catenin (102 kDa) used as normalizer. Inset shows longer exposure of the Gli3^{A} band. Asterisk indicates a non-specific protein (80 kDa) reacting with the antibody. (F1-H2) In situ hybridization using ^{35}S-labeled riboprobes against *Gli1* (F1,F2), *Gli2* (G1,G2) and *Gli3* (H1,H2) on longitudinal sections through the ulna (F1,F2,H1,H2) or the humerus (G1,G2) from E14.5 wild type (F1-H1) or *Ihh*$^{-/-}$ (F2-H2) embryos. Shown is the distal region of each element. Green arrows indicate expression in the perichondrium. Green asterisks indicate the periarticular region. P, proliferative chondrocytes; H, hypertrophic chondrocytes. r, h, u (F2,H2) indicate radius, humerus and ulna, respectively.

proximal elements such as the humerus (‘h’) (Fig. 1A3) and the femur (‘f’) (Fig. 1B3) in the DKO embryo contained some abnormal bone (green arrowheads in insets) around the mineralized cartilage at the diaphysis of these elements. Overall, bone formation remained largely dysregulated in the DKO embryo.

The DKO embryo exhibited additional rescue phenotypes in the rest of the skeleton. The rib cage that was characteristically diminished in the *Ihh*$^{-/-}$ embryo (Fig. 1C2) was restored in the DKO embryo (Fig. 1C3) to a similar size to wild type (Fig. 1C1). Notably, the sternum of the DKO embryo was not fused (asterisk, Fig. 1C3), a feature characteristic of the *Gli3*$^{-/-}$ mutant (Fig. 1C4) but not that of the *Ihh*$^{-/-}$ embryo (Fig. 1C2). Moreover, the *Ihh*$^{-/-}$ mutant typically exhibited a ‘dome-shaped’ skull, and a shortened snout (Fig. 1D2), and these features were largely corrected in the DKO embryo (Fig. 1D3). Importantly, the chondrocranium of the DKO embryo was noticeably bigger than its *Ihh*$^{-/-}$ counterpart but similar to the wild-type size (asterisks, Fig. 1D1-D3). Thus, normalization of cartilage development may be responsible for the rescue phenotype in the skeleton of the DKO embryo.

We next determined whether Ihh antagonizes Gli3 activity

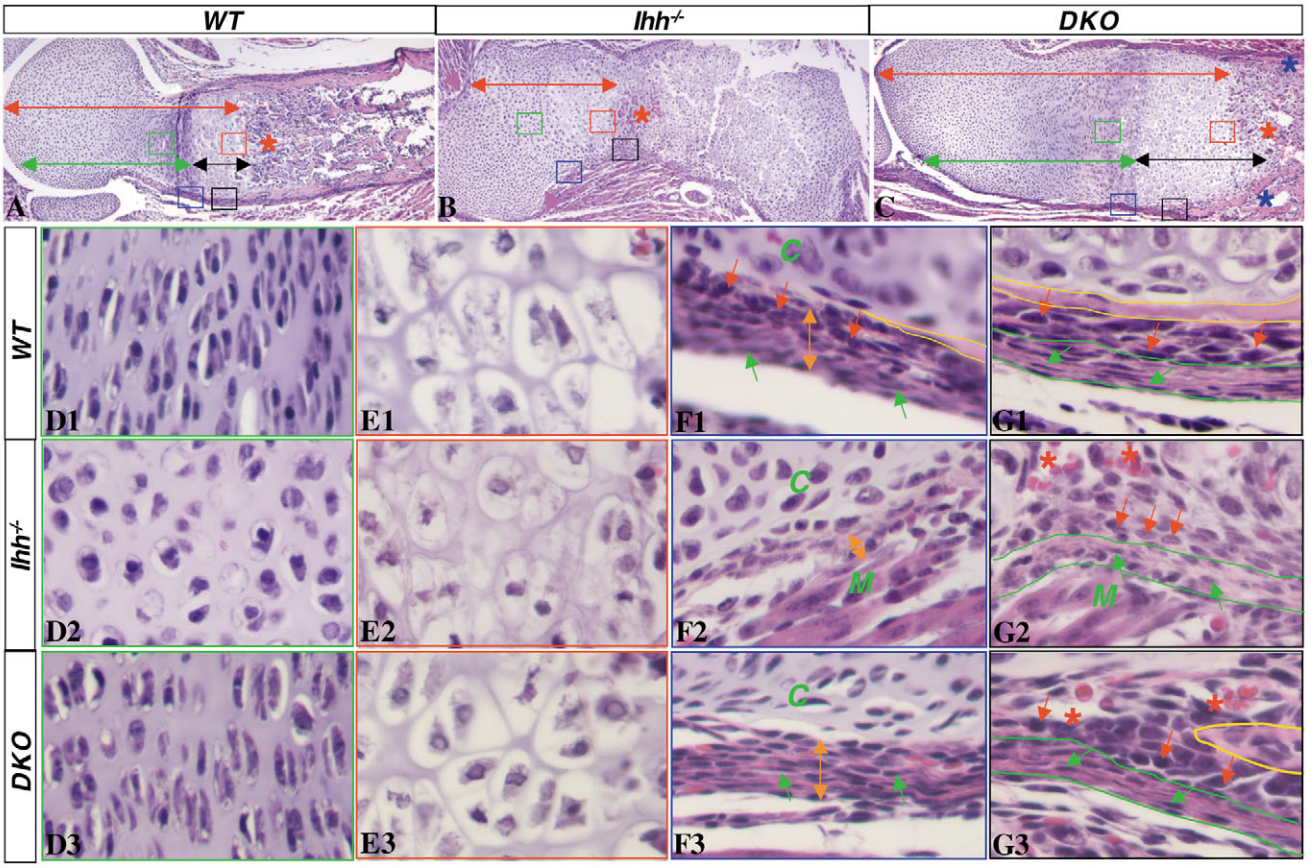

Fig. 2. Restoration of chondrocyte morphology and perichondrium growth in the humerus of the DKO embryo at E18.5. (A-C) Low-magnification images of Hematoxylin and Eosin stained sections from the wild type (A), *Ihh*$^{-/-}$ (B) and DKO (C) embryos. Red arrows indicate the entire growth region. Green and black arrows (A,C) mark the non-hypertrophic, and the hypertrophic regions, respectively. Asterisks indicate areas of vascularization. Rectangle boxes of different colors identify various areas shown at a higher magnification below. (D1-D3,E1-E3,F1-F3,G1-G3) Images at a higher magnification of areas in A-C that are boxed in different colors: green, red, blue and black respectively. Red and green arrows (F1,F3,G1-G3) indicate cuboidal and elongated cells, respectively. Double-headed arrows (F1-F3) indicate width of perichondrium. C (F1-F3), chondrocytes; M (F2,G2), muscle. Yellow contours (F1,G1,G3) indicate the bone collar. Green lines (G1-G3) demarcate the outer layers of the perichondrium. Asterisks (G2,G3) indicate areas of vascularization.

by regulating the proteolytic processing of Gli3. Western analyses were performed with whole cell lysates harvested from E14.5 limb cartilage, using a Gli3 antibody. Although the truncated repressor form of Gli3 (Gli3^{R}, 83 kDa) was detectable in the normal cartilage (Fig. 1E, 'WT'), its amount was much increased in the absence of *Ihh* (Fig. 1E, '*Ihh*$^{-/-}$'). Interestingly, in both the wild type and the *Ihh*$^{-/-}$ cartilage, the full-length activator form (Gli3^{A}, 190 kDa) was a minor form that could be detected only after longer exposure (Fig. 1E, inset). Moreover, the total amount of Gli3 in the *Ihh*$^{-/-}$ cartilage appeared to more than that in the wild-type cartilage. Thus, the loss of Ihh likely resulted in an increase in both Gli3 total production as well as the relative levels of Gli3^{R}. The specificity of the Gli3^{R} and Gli3^{A} bands was confirmed by their absence in the *Gli3*$^{-/-}$ sample (Fig. 1E, '*Gli3*$^{-/-}$'). A non-specific 80 kDa band also recognized by the antibody was conveniently used as a loading control (asterisk, Fig. 1E). The similar loading across the genotypes was confirmed by using an antibody against α-catenin, an abundant adherens junction protein (Fig. 1E).

The apparent increase in total Gli3 production in the *Ihh*$^{-/-}$ embryo prompted us to examine its expression level in the mutant versus wild-type embryo by in situ hybridization. At E14.5 in a wild-type embryo (Fig. 1H1), *Gli3* was expressed by the proliferative chondrocytes ('P'), in the perichondrium (green arrows) as well as at the periarticular region (asterisk). In the *Ihh*$^{-/-}$ embryo, *Gli3* levels in all domains appeared to be elevated (Fig. 1H2). On the contrary, *Gli1*, which was expressed in similar domains as *Gli3* in the wild-type embryo, was undetectable in the *Ihh*$^{-/-}$ littermate (compare Fig. 1F1 with F2). Finally, *Gli2* was normally expressed in the perichondrium (green arrows) as well as the proliferating chondrocytes ('P') (Fig. 1G1), and maintained a similar expression level in these domains in the *Ihh*$^{-/-}$ embryo, although the proliferative zone was much diminished in the mutant humerus (Fig. 1G2). Curiously, *Gli2* expression in the periarticular region appeared to be elevated in the *Ihh*$^{-/-}$ embryo (asterisk, Fig. 1G2). Thus, all three *Gli* molecules were expressed in the developing long bones and *Gli3* expression was elevated in the absence of Ihh.

Normal proliferation and maturation of chondrocytes in the DKO embryo

Results from the whole-mount skeleton analyses prompted us

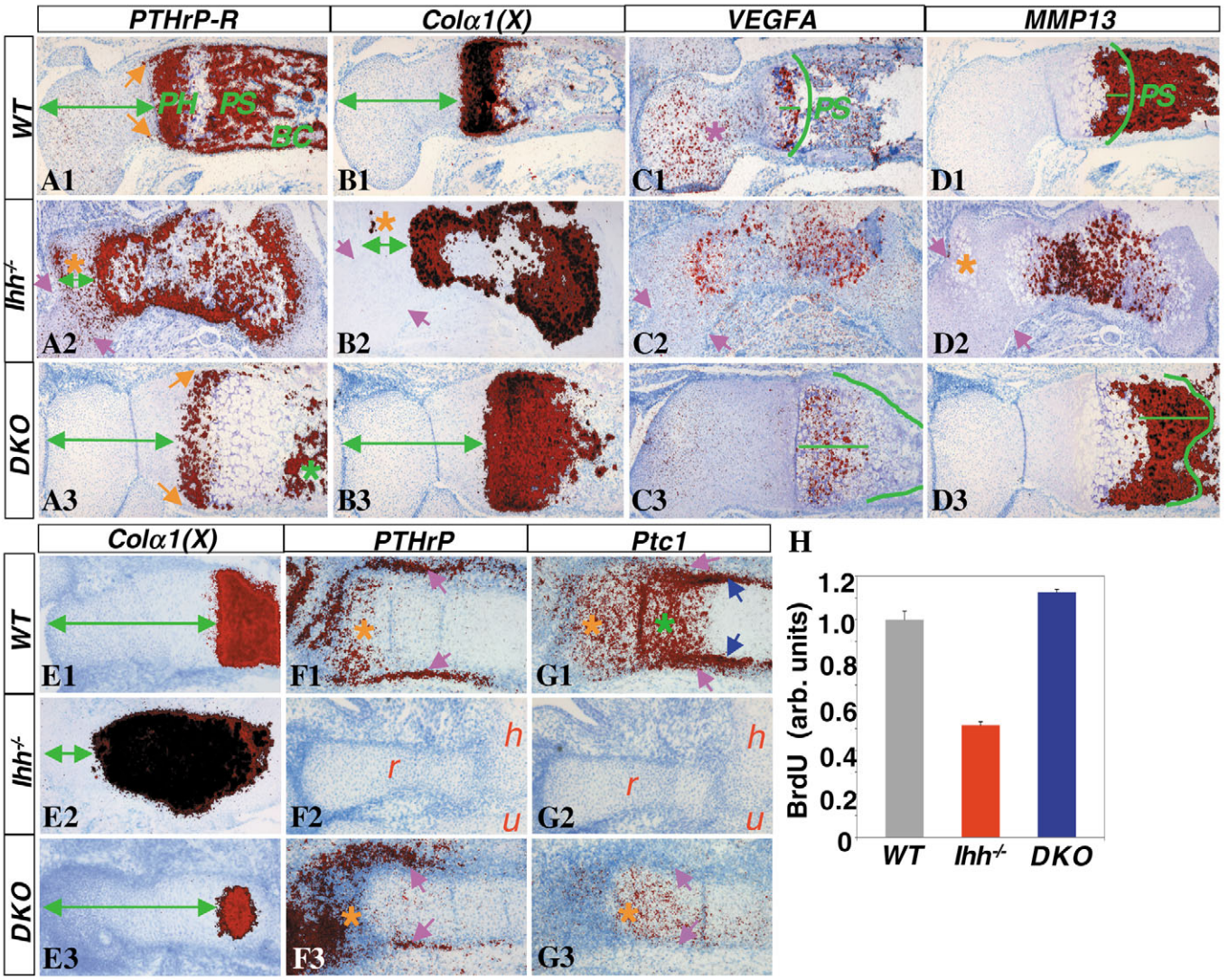

Fig. 3. Molecular analyses of chondrocyte maturation, and chondrocyte proliferation assays. (A1-A3,B1-B3,C1-C3,D1-D3) In situ hybridization using ^{35}S-labeled riboprobes against *Pthr* (A1-A3), *Col10a1* (B1-B3), *Vegfa* (C1-C3) and *Mmp13* (D1-D3), on longitudinal sections through the humerus from E18.5 embryos of wild type (A1-D1), *Ihh*$^{-/-}$ (A2-D2) or DKO (A3-D3). Shown are the distal halves of the humerus for the wild type (A1-D1) and the DKO (A3-D3) embryo, but the full length for the *Ihh*$^{-/-}$ embryo (A2-D2). Hybridization signals are in red. Double-headed arrows (A1-A3,B1-B3) denote zones of immature chondrocytes. Yellow arrows (A1,A3) indicate the perichondrium. Purple arrows (A2-D2) indicate joint fusion with the radius. Yellow asterisks (A2,B2,D2) indicate ectopic hypertrophy of chondrocytes. Purple asterisk (C1) indicates immature chondrocytes. Green asterisk (A3) indicates ectopic bone. PH (A1), prehypertrophic chondrocytes; PS (A1,C1,D1), primary spongiosa; BC (A1), bone collar. Green straight lines (C1,C3,D1,D3) demarcate sub-domains of the hypertrophic zone. Green contours denote the boundary between the hypertrophic cartilage and either the primary spongiosa (C1,D1) or the ectopic bone (C3,D3). (E1-G3) In situ hybridization using ^{35}S-labeled riboprobes against *Col10a1* (E1-E3), *Pthlh* (F1-F3) and *Ptc1* (G1-G3), on longitudinal sections from E14.5 embryos of wild type (E1-G1), *Ihh*$^{-/-}$ (E2-G2) or DKO (E3-G3), through either the humerus (E1-E3) or the radius (F1-F3,G1-G3). Hybridization signals are in red. Shown are the distal halves of the humerus or the radius for the wild type (E1-G1) and the DKO (E3-G3) embryo, but the full length of either element for the *Ihh*$^{-/-}$ embryo (E2-G2). Double-headed arrows (E1-E3) indicate zones of immature chondrocytes. Purple arrows (F1,F3,G1,G3) and blue arrows (G1) indicate the outer and inner layers of the perichondrium, respectively. Yellow asterisks (F1,F3,G1,G3) indicate periarticular chondrocytes. Green asterisk (G1) denotes immature chondrocytes adjacent to the prehypertrophic zone. r, h, u (F2,G2): radius, humerus and ulna, respectively. (H) BrdU labeling index for chondrocytes in the humerus (distal half) of E14.5 embryos of wild type (WT), *Ihh*$^{-/-}$ and DKO. The wild-type value is arbitrarily assigned 1.

to examine first whether cartilage development was normalized in the DKO embryo. We first analyzed chondrocyte maturation by histological analyses. At E18.5, the *Ihh*$^{-/-}$ embryo exhibited only very rudimentary vascularization at the center of the humerus (asterisk, Fig. 2B) and contained a much reduced growth region (red double-headed arrow, Fig. 2B) as previously described (St-Jacques et al., 1999). By contrast, in the DKO embryo vascularization was more advanced (asterisk, Fig. 2C), and the growth region was markedly increased (red double-headed arrow, Fig. 2C). Interestingly, both the

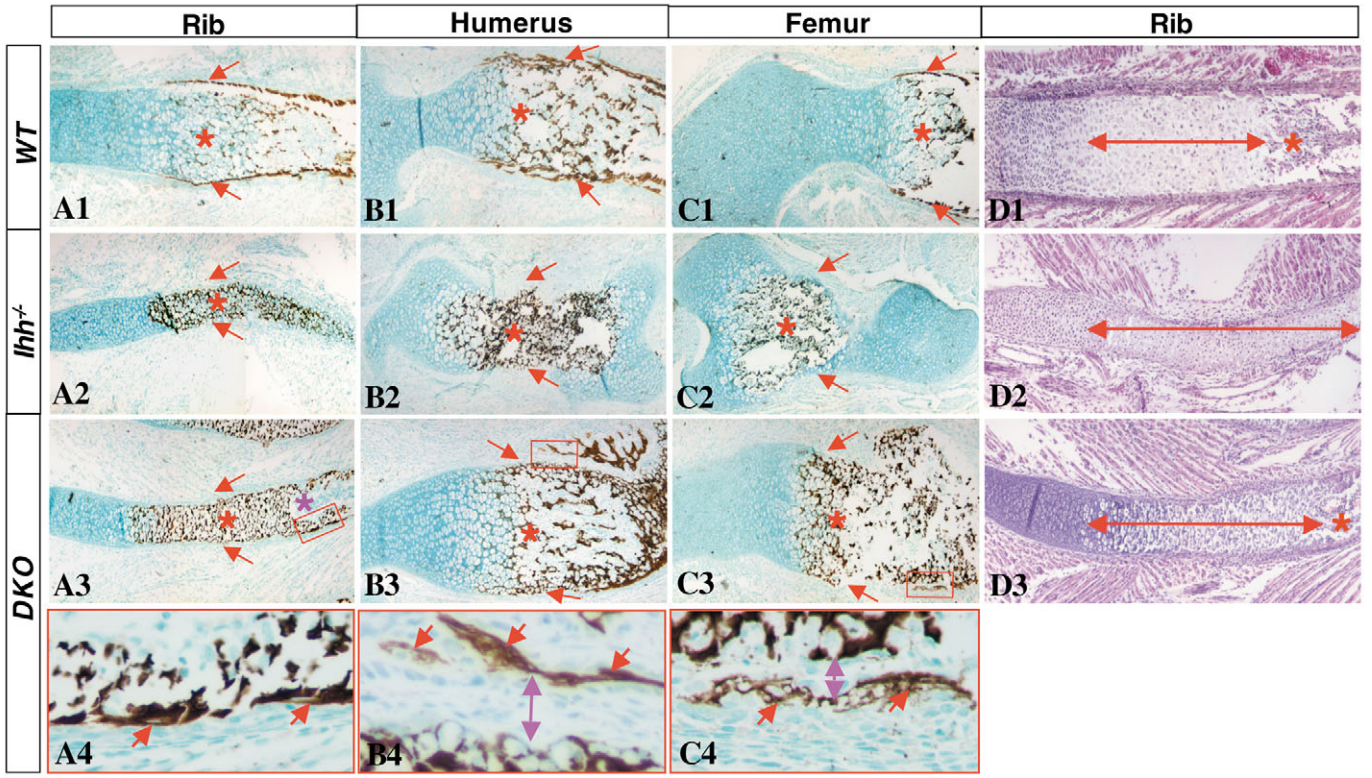

Fig. 4. Defects in bone formation and cartilage vascularization in the DKO embryo. (A1-A4,B1-B4,C1-C4) Von kossa staining on longitudinal sections of the ribs (A1-A4), the humeri (B1-B4) and the femurs (C1-C4) from E18.5 embryos of wild type (A1-C1), *Ihh*$^{-/-}$ (A2-C2) and DKO (A3-C3,A4-C4). (A1-A3,B1-B3,C1-C3) Images at a low magnification. The ribs (A1-A3) were oriented with the ventral side towards the left, and the humeri (B1-B3) and the femurs (C1-C3) the distal end towards the left. Arrows denote either the normal bone collar (A1-C1), or the corresponding perichondrium where the bone collar is missing (A2-C2,A3-C3). Red asterisks, mineralized cartilage; purple asterisk (A3), marrow cavity. (A4-C4) Images at a higher magnification of boxed areas in A3-C3, respectively. Arrows indicate ectopic bone. Double-headed arrows (B4,C4) indicate the perichondrium separating the ectopic bone from mineralized cartilage. (D1-D3) Hematoxylin and Eosin staining of sections through the equivalent ribs from E18.5 embryos of wild type (D1), *Ihh*$^{-/-}$ (D2) and DKO (D3). Double-headed arrows indicate the length of the hypertrophy zone. Asterisks (D1,D3) indicate areas of vascularization.

nonhypertrophic (green double-headed arrow) and the hypertrophy zone (black double-headed arrow) were widened in the DKO embryo over the wild-type counterpart (Fig. 2, compare A and C), suggesting likely delays in both the onset and the removal of hypertrophic chondrocytes in the DKO embryo.

Examination at a higher magnification revealed a rescue of the organization of the growth region chondrocytes in the DKO embryo. In the wild-type embryo at E18.5, stacks of flattened cells (Fig. 2D1) arranged in columns (columnar chondrocytes) preceded the hypertrophic chondrocytes (Fig. 2E1) that became fully vacuolated prior to their removal at the chondro-osseous junction. In the *Ihh*$^{-/-}$ embryo, chondrocytes were severely disorganized so that no stacks of cells were evident (Fig. 2D2). Moreover, although a majority of chondrocytes have undergone hypertrophy in the *Ihh*$^{-/-}$ embryo at E18.5 (St-Jacques et al., 1999), the 'hypertrophic' chondrocytes here were noticeably smaller than the wild-type counterparts (Fig. 2E2). Remarkably, in the DKO embryo, both columnar chondrocytes (Fig. 2D3) and the hypertrophy phenotype (Fig. 23E) were fully restored. Thus, chondrocyte organization and maturation at the growth region was normalized in the DKO embryo.

Analyses of the histological sections also revealed differences in the perichondrium among the various embryos. In the wild-type embryo, concurring with chondrocyte development, the perichondrium also underwent distinct morphological changes along the epiphyseal-diaphyseal axis. Specifically, in regions flanking the prehypertrophic chondrocytes (Fig. 2F1), the perichondrium (orange double-headed arrows) differentiated into an inner region with more and cuboidal cells (red arrows) contrasting with an outer region with fewer and elongated cells (green arrows). The morphological distinction between the layers became more pronounced in regions flanking the hypertrophy zone (Fig. 2G1) where the inner layer containing cuboidal cells (red arrows) directly lined the bone collar (yellow contour), whereas the outer layer (green contour) became more fibrous and contained fewer and much elongated cells (green arrows). In the *Ihh*$^{-/-}$ embryo, the perichondrium was generally hypoplastic (orange double-headed arrow, Fig. 2F2). At the diaphysis where rudimentary vascularization occurred (Fig. 2G2), although the perichondrium thickened with more cuboidal cells (red arrows) in the inner region and more elongated cells (green arrows) in the outer region (green contour), no distinct layers were established. In the DKO embryo, the width of the perichondrium (orange double-headed arrow, Fig. 2F3) was markedly increased over the *Ihh*$^{-/-}$

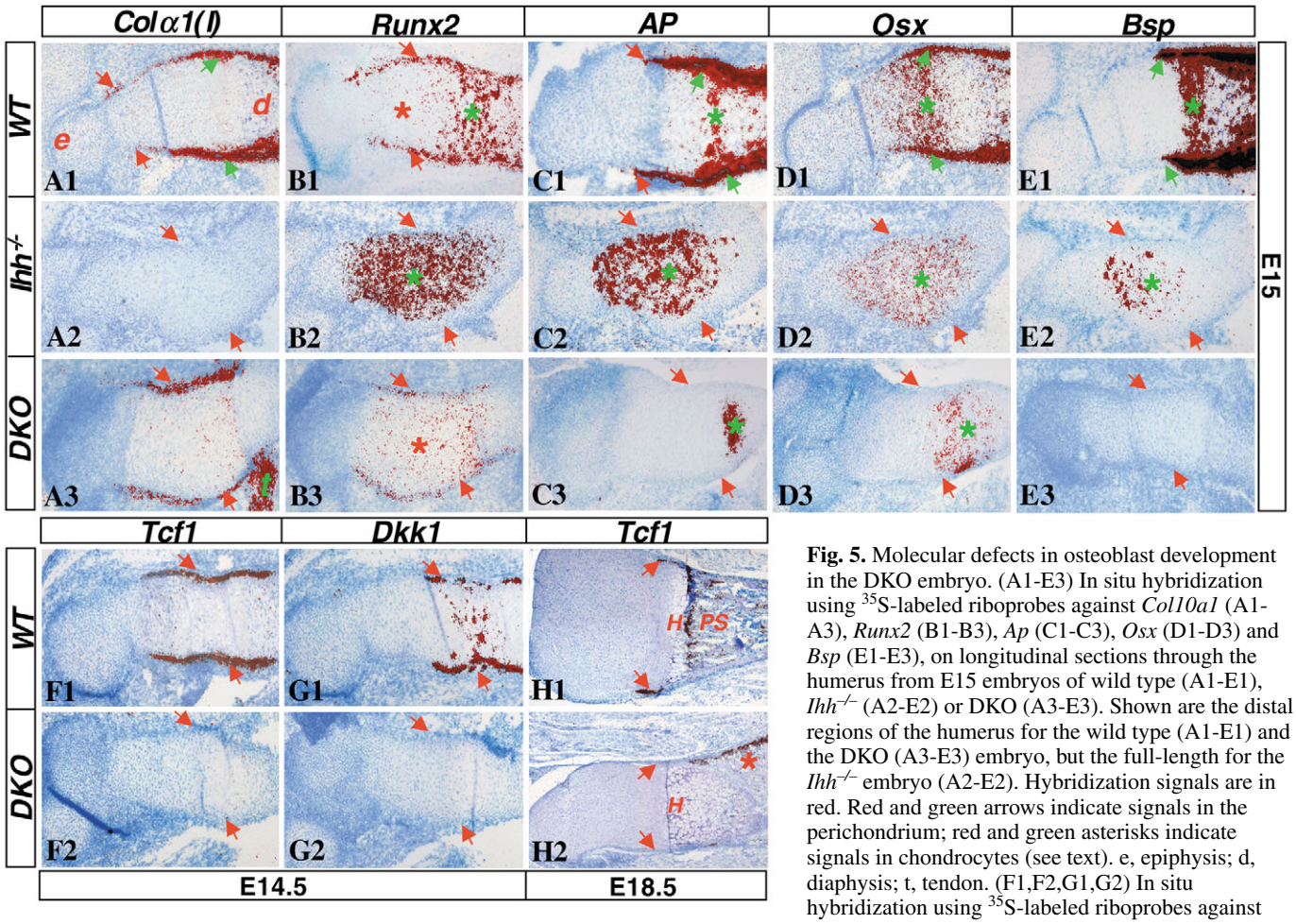

Fig. 5. Molecular defects in osteoblast development in the DKO embryo. (A1-E3) In situ hybridization using ^{35}S-labeled riboprobes against *Col10a1* (A1-A3), *Runx2* (B1-B3), *Ap* (C1-C3), *Osx* (D1-D3) and *Bsp* (E1-E3), on longitudinal sections through the humerus from E15 embryos of wild type (A1-E1), *Ihh*$^{-/-}$ (A2-E2) or DKO (A3-E3). Shown are the distal regions of the humerus for the wild type (A1-E1) and the DKO (A3-E3) embryo, but the full-length for the *Ihh*$^{-/-}$ embryo (A2-E2). Hybridization signals are in red. Red and green arrows indicate signals in the perichondrium; red and green asterisks indicate signals in chondrocytes (see text). e, epiphysis; d, diaphysis; t, tendon. (F1,F2,G1,G2) In situ hybridization using ^{35}S-labeled riboprobes against *Tcf1* (F1,F2) and *Dkk1* (G1,G2) on longitudinal sections through the humerus from E14.5 wild type (F1-G1) and DKO (F2,G2) embryos. Shown are the distal regions of the humerus. Red arrows indicate the perichondrium. (H1,H2) In situ hybridization using ^{35}S-labeled riboprobes against *Tcf1* on longitudinal sections through the humerus from E18.5 embryos of wild type (H1) and DKO (H2). Red arrows indicate either signals in the perichondrium (H1) or the corresponding regions missing the signals (H2). Red asterisk (H2) indicates the ectopic bone. H, hypertrophic zone; PS, primary spongiosa.

mutant and was similar to the wild-type counterpart. However, in contrast to that in the wild-type embryo, the perichondrium flanking the prehypertrophic chondrocytes in the DKO animal failed to differentiate into the morphologically distinct layers, but instead was uniformly populated with elongated cells (green arrows, Fig. 2F3). Differentiation of the perichondrium eventually occurred around the mid-region of the hypertrophic zone where bone formation began to occur (yellow contour, Fig. 2G3). Here, as in the wild-type animal, the cuboidal cells (red arrows) resided immediately adjacent to the bone collar, whereas the elongated cells (green arrows) populated the outer fibrous layer (green contour). Thus, the perichondrium in the DKO embryo exhibited normal growth but failed to undergo normal differentiation.

To confirm that chondrocyte maturation was rescued in the DKO embryo, we next examined the expression of chondrocyte maturation markers by in situ hybridization. At E18.5, in the wild-type humerus, parathyroid hormone-related peptide receptor (*Pthr*) was highly expressed in the prehypertrophic chondrocytes ('PH', Fig. 3A1), in addition to expression in the osteoblast lineage as detected in the primary spongiosa ('PS'), the bone collar ('BC') as well as the perichondrium (orange arrows). Type X collagen (*Col10a1*) was specifically expressed in all hypertrophic chondrocytes (Fig. 3B1). Within the hypertrophic zone, vascular endothelial growth factor A (*Vegfa*) exhibited a high level expression in the mid-region hypertrophic chondrocytes (green line, Fig. 3C1), whereas matrix metalloproteinase 13 (*Mmp13*) was largely restricted to the late hypertrophic chondrocytes (green line, Fig. 3D1). *Vegfa* was also detected at a lower level throughout the core of the immature cartilage (purple asterisk, Fig. 3C1), whereas *Mmp13* was also expressed in cells associated with the primary spongiosa ('PS', Fig. 3D1). As previously documented, at E18.5 the *Ihh*$^{-/-}$ embryo exhibited precocious maturation of chondrocytes, as evidenced by the close proximity of prehypertrophic (*Pthlh* positive) and hypertrophic (*Col10a1* positive) cells to the epiphysis (note reduced lengths of green double-headed arrows, Fig. 3A2,B2). Accordingly, cells expressing *Vegfa* (Fig. 3C2) and *Mmp13* (Fig. 3D2) were also closer to the epiphysis (demarcated by purple arrows, contiguous with radius because of joint fusion). Moreover, the linear progression of chondrocyte maturation from diaphysis

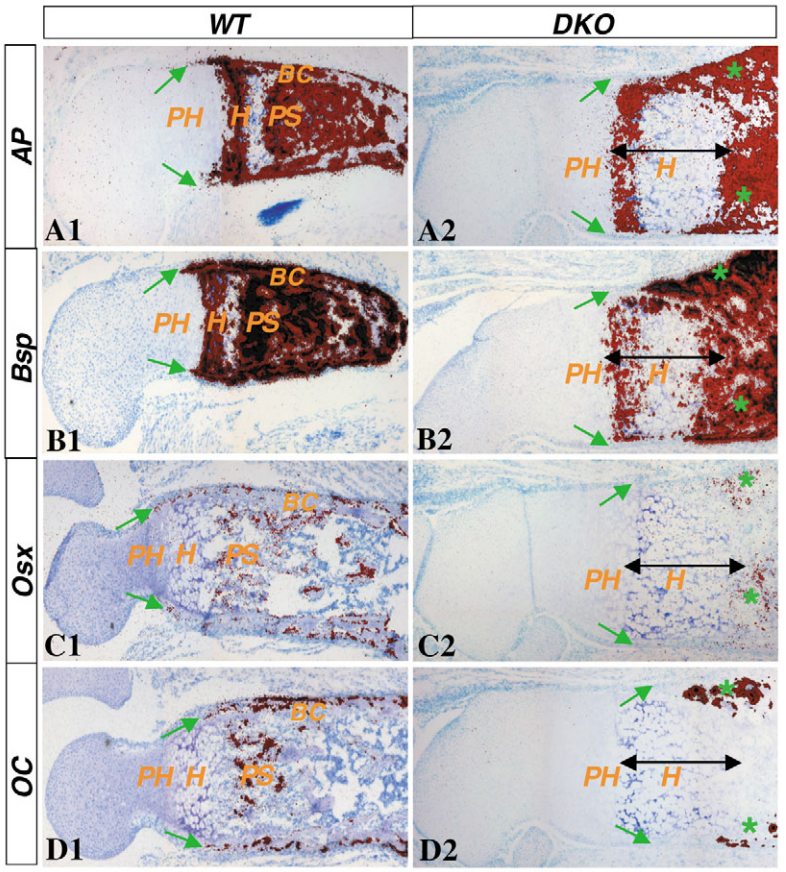

Fig. 6. Lack of orthotopic bone formation at E18.5. In situ hybridization using ^{35}S-labeled riboprobes against *Ap* (A1,A2), *Bsp* (B1,B2), *Osx* (C1,C2) and *Oc* (D1,D2), on longitudinal sections through the humerus from E18.5 wild type (A1-D1) and DKO (A2-D2) embryos. Shown are the distal halves of the humerus. Green arrows indicate either signals in the perichondrium (A1-D1) or the corresponding regions missing the signals (A2-D2). Black double-headed arrows (A2-D2) indicate the widened hypertrophy zone. Green asterisks (A2-D2) indicate the ectopic bone. BC, bone collar; PH, prehypertrophic zone; H, hypertrophic zone; PS, primary spongiosa.

to epiphysis was disrupted in the *Ihh*$^{-/-}$ embryo, as the maturation markers were expressed in a concentric fashion (Fig. 3A2-D2). By contrast, in the DKO embryo expression of all markers was restored to largely normal domains (Fig. 3A3-D3). Consistent with the histological results (above), both the immature (green double-headed arrows, Fig. 3A3,B3) and the hypertrophic (*Col10a1* positive, Fig. 3B3) zones were widened over the wild-type counterparts. Importantly, the domains expressing later hypertrophic makers such as *Vegfa* (green line, Fig. 3C3) and *Mmp13* (green line, Fig. 3D3) were markedly expanded in the DKO embryo, consistent with a delay in the removal of late hypertrophic chondrocytes. The widened zone for immature chondrocytes reflected a delay in maturation in the DKO embryo, and this was most evident in the humerus at E14.5, when the DKO embryo showed a clear retardation in *Col10a1* expression (Fig. 3, compare E1 with E3), in contrast to the *Ihh*$^{-/-}$ embryo where *Col10a1* expression was much accelerated (Fig. 3E2). Overall, molecular analyses confirmed that proper chondrocyte maturation was largely restored in the DKO embryo.

Restoration of proper chondrocyte maturation in the DKO embryo prompted us to examine the expression of *Pthlh*. Pthlh has previously been shown to be a principal regulator of chondrocyte maturation functioning as a secondary signal for Ihh (Karp et al., 2000; Lanske et al., 1996; Vortkamp et al., 1996). At E14.5, the wild-type radius expressed high levels of *Pthlh* both in the periarticular chondrocytes (yellow asterisk) and in the outer layers of perichondrium flanking the immature chondrocytes (purple arrows, Fig. 3F1). These regions corresponded to a low level of patched 1 (*Ptch1*) expression (yellow asterisk and purple arrows, Fig. 3G1) but were distinct from domains expressing high levels of *Ptch1* (green asterisk and blue arrows, Fig. 3G1). As previously reported, *Pthlh* expression was abolished in the developing cartilage of *Ihh*$^{-/-}$ embryos (Fig. 3F2), similar to the elimination of *Ptch1* expression (Fig. 3G2). Remarkably, in the DKO embryo *Pthlh* expression was fully restored in both the periarticular (yellow asterisk) and the perichondrium region (purple arrows, Fig. 3F3). Similarly, a low level of *Ptch1* expression was detected in both the immature chondrocytes (yellow asterisk) and the perichondrium (purple arrows, Fig. 3G3) in the DKO embryo, whereas the high level *Ptch1* expression was not restored. In summary, both *Pthlh* and a low level of *Ptch1* expression were rescued in the cartilage of the DKO embryo.

We next examined the status of chondrocyte proliferation in the growth region cartilage. BrdU labeling experiments showed that the proliferation rate of chondrocytes in E14.5 DKO embryos was similar to the wild-type level, in contrast to a 50% reduction in *Ihh*$^{-/-}$ embryos (Fig. 3H).

Bone formation correlated with a partial rescue of vascularization in DKO embryos

The whole-mount skeletal staining experiment above revealed abnormal bone formation in certain skeletal elements of the DKO embryo. To confirm this finding, we stained tissue sections by the von Kossa method. At E18.5, the wild-type embryo had developed a definitive bone collar (arrows) surrounding the mineralized cartilage (red asterisks) in the long bones such as the ribs (Fig. 4A1), the humerus (Fig. 4B1) and the femur (Fig. 4C1). The *Ihh*$^{-/-}$ embryo, however, as previously reported, completely lacked the bone collar (arrows) in all long bones although cartilage mineralization occurred (asterisks, Fig. 4A2-C2). Like the *Ihh*$^{-/-}$ embryo, the DKO embryo also lacked a bone collar at the normal position in all long bones (arrows, Fig. 4A3-C3) despite ample mineralization in the cartilage (red asterisks, Fig. 4A3-C3). Interestingly, however, in the humerus (Fig. 4B3 and B4) and the femur (Fig. 4C3 and C4), as well as certain ribs (Fig. 4A3 and A4), a varying amount of bone deposition (arrows, Fig. 4A4-C4) was detected at the diaphysis. A similar observation was made in the ulna (data not shown). The bone deposition was often asymmetrical and not adherent to the underlying cartilage (double-headed arrows, Fig. 4B4,C4). An additional important feature of the ectopic bone was that it invariably

correlated with vascularization of the cartilage, as evidenced by the presence of red blood cells (purple asterisk, Fig. 4A3). Moreover, the degree of ossification also correlated with that of vascularization. For example, the humerus (Fig. 4B3) often exhibited more ossification and was also more advanced in vascularization, whereas the femur (Fig. 4C3) lagged in both aspects. Thus, in the DKO embryo, the normal bone collar failed to form but ectopic bone developed at the diaphysis of long bones where vascularization occurred.

Cartilage vascularization in the long bones of the DKO embryo was partially rescued over the *Ihh*$^{-/-}$ embryo, although it remained defective compared with the wild-type embryo. This was exemplified in a rib of an E18.5 DKO embryo by the appearance of a rudimentary marrow cavity (red asterisk, Fig. 4D3), whereas no vascularization was noted in any ribs of an *Ihh*$^{-/-}$ embryo at same age (Fig. 4D2). The vascularization in the DKO embryo was noticeably delayed compared to the wild-type embryo, resulting in a wider hypertrophic zone (Fig. 4, double-headed arrows, compare D1 with D3).

A partial rescue of orthotopic osteoblast development in DKO embryos

The lack of normal bone collars in the DKO embryo prompted us to investigate in detail the development of the osteoblast lineage. To this end, we examined the expression of a panel of markers activated at various stages of osteoblast development. At E15, in a wild-type humerus, *Runx2* as well as low levels of *Col10a1* and alkaline phosphatase (*Ap*; *Akp* – Mouse Genome Informatics) were characteristically expressed in the perichondrial cells (red arrows, Fig. 5A1-C1) towards the epiphysis (‘e’, Fig. 5A1), representing early stages of the osteoblast lineage. Towards the diaphysis (‘d’, Fig. 5A1) where cells of the lineage became progressively more mature, the levels of *Col10a1* and *Ap* were elevated in the perichondrium (green arrows, Fig. 5A1,C1), whereas *Runx2* expression (green arrow, Fig. 5B1) remained relatively constant. Meanwhile, *Osx* (*Sp7* – Mouse Genome Informatics) and subsequently bone sialoprotein (*Bsp*) were activated in the more mature perichondrium (green arrows, Fig. 5D1,E1). In addition to the expression in the osteoblast lineage, high levels of *Runx2*, *Ap* and *Bsp* were also detected in hypertrophic chondrocytes (green asterisks, Fig. 5B1,C1,E1, respectively), whereas *Osx* was also in the prehypertrophic cells (green asterisk, Fig. 5D1). Moreover, a lower level of *Runx2* was also detected in the immature chondrocytes (red asterisk, Fig. 5B1). In the *Ihh*$^{-/-}$ embryo, consistent with previous reports (Hu et al., 2005; St-Jacques et al., 1999), none of the osteoblast markers were expressed in the perichondrium at E15 (red arrows, Fig. 5A2-E2), although a number of molecules were diffusedly expressed in the cartilage, reflecting the dysregulation of chondrocyte maturation (green asterisks, Fig. 5B2-E2). Interestingly in the DKO embryo, although *Col10a1* and *Runx2* were expressed in the perichondrium (red arrows, Fig. 5A3,B3, respectively), *Ap*, *Osx* or *Bsp* could not be detected there (red arrows, Fig. 5C3-E3, respectively). Moreover, the level of *Col10a1* expression remained low throughout the perichondrium (red arrows, Fig. 5A3). In the cartilage, expression of *Ap* and *Osx* (green asterisks, Fig. 5C3 and D3, respectively) became restricted to discrete domains similar those in the wild-type embryo. *Bsp* and high levels of *Runx2*, both characteristic of later hypertrophic chondrocytes, were not yet expressed in the cartilage at this stage (Fig. 5D3 and B3, respectively), consistent with a delay in chondrocyte maturation in the DKO embryo, as noted earlier. However, similar to the wild-type embryo, a low level of *Runx2* expression was detected in the immature chondrocytes in the DKO embryo (red asterisk, Fig. 5B3). Thus, development of the osteoblast lineage was initiated but was later stalled in the DKO embryo.

We next further investigated the molecular basis for the arrest of osteoblast development in the DKO embryo. Our previous work identified that Wnt signaling through the canonical pathway was crucial for osteoblast development and that this signaling was abolished in the *Ihh*$^{-/-}$ embryo (Hu et al., 2005). We therefore examined whether canonical Wnt signaling was rescued in the DKO embryo. At E14.5, in the wild-type embryo *Tcf1* and *Dkk1*, both direct transcriptional targets of Wnt canonical signaling (Chamorro et al., 2005; Gonzalez-Sancho et al., 2005; Niida et al., 2004; Roose et al., 1999), were upregulated in the perichondrium (red arrows, Fig. 5F1,G1). In the DKO embryo, however, as in the *Ihh*$^{-/-}$ mutant (Hu et al., 2005), *Tcf1* and *Dkk1* were not detected in the perichondrial cells (Fig. 5F2,G2, respectively). Importantly, the canonical Wnt pathway remained quiescent even at E18.5, when *Tcf1* was normally expressed in the perichondrium flanking the prehypertrophic chondrocytes (red arrows, Fig. 5H1) but was not detectable in a similar region in the DKO embryo (red arrows, Fig. 5H2). Notably, *Tcf1* expression was activated in the periosteum overlying the ectopic bone (asterisk, Fig. 1H2), indicating that canonical Wnt signaling was coupled with bone formation at the ectopic site. Thus, in the DKO embryo, osteoblast development at the orthotopic position was arrested prior to the activation of canonical Wnt signaling in the progenitors.

We next investigated whether the defect in orthotopic osteoblastogenesis was merely a temporary delay that was corrected at later stages. At E18.5, in the wild type humerus *Ap* and *Bsp* (Fig. 6A1,B1, respectively) were expressed highly in cells of the osteoblast lineage associated with the primary spongiosa (‘PS’), the bone collar (‘BC’) as well as the perichondrium (green arrows) flanking the prehypertrophic chondrocytes (‘PH’), in addition to their expression in the hypertrophic chondrocytes (‘H’). Similarly, *Osx* (Fig. 6C1) was expressed in the primary spongiosa (‘PS’), the bone collar (‘BC’) and the perichondrium (arrows). Osteocalcin (*Oc*; *Bglap1* – Mouse Genome Informatics) (Fig. 6D1), a specific marker for the mature osteoblast, was detected in the primary spongiosa (‘PS’) as well as the bone collar (‘BC’) that extended to flank the mid-region (green arrows) of the hypertrophic zone (‘H’). By contrast, in the DKO humerus (Fig. 6A2-D2) none of the markers were detected in the corresponding regions of the perichondrium (green arrows), indicating a persistent lack of orthotopic bone formation. However, all the markers were expressed in the ectopic bone formed around the diaphysis (green asterisks, Fig. 6A2-D2). Thus, orthotopic osteoblast development was persistently arrested in the DKO embryo, even though ectopic bone formed at the diaphysis.

Distinct fates for perichondrial mesenchymal cells in the absence of either Ihh or canonical Wnt signaling

Our earlier observation that less bone formed at the femur than

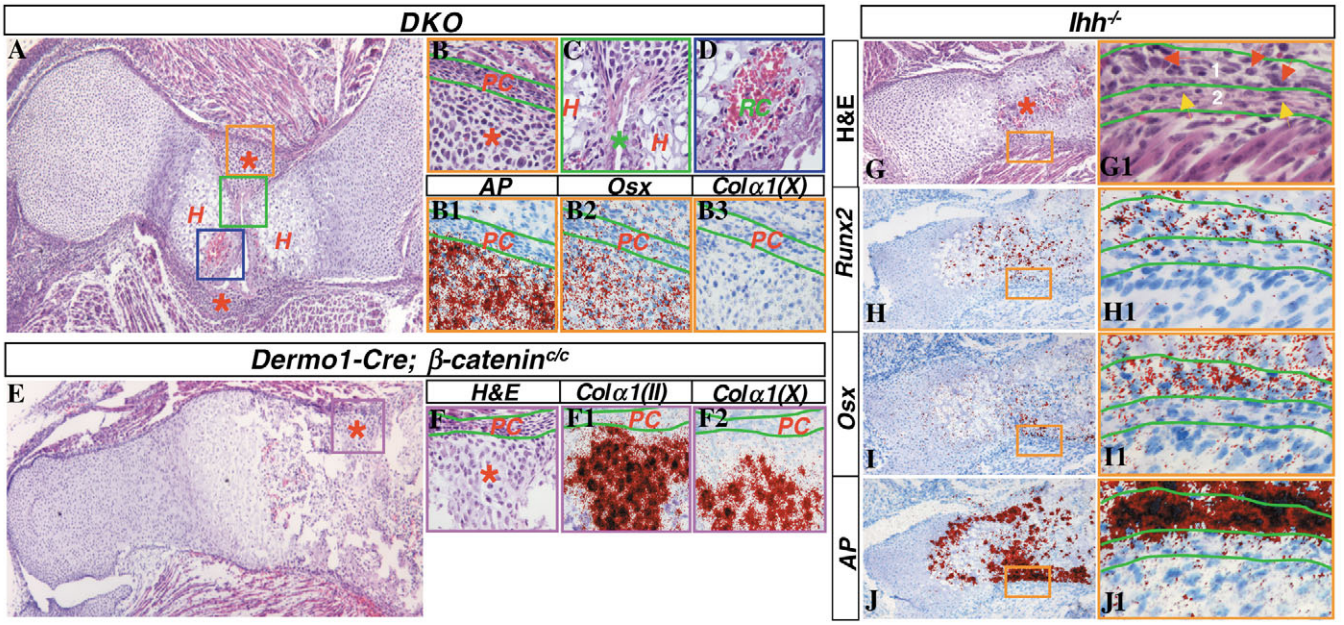

Fig. 7. Osteoblast versus chondrocyte differentiation from the perichondrial progenitors. (A-D) Histology of the femur from an E18.5 DKO embryo. Areas in yellow, green and blue boxes (in A) are shown at a higher magnification in B-D, respectively. H, hypertrophy zone; PC, perichondrium; RC, red blood cells. Red asterisks in A,B indicate mesenchymal cells; green asterisk in C marks the death zone. (B1-B3) In situ hybridization using ^{35}S-labeled riboprobes against *Ap* (B1), *Osx* (B2) and *Col10a1* (B3), on sections adjacent to that in A. Areas similar to that in B are shown at the same magnification. Hybridization signals are in red. PC, perichondrium. (E,F) Histology of the humerus from an E18.5 *Dermo1-Cre; β-catenin$^{c/c}$* embryo. Area in purple box (E) is shown at a higher magnification (F). Asterisks in E,F indicate ectopic chondrocytes. (F1,F2) In situ hybridization using ^{35}S-labeled riboprobes against *Col2a1* (F1) and *Col10a1* (F2), on sections adjacent to that in E. Areas similar to that in F are shown at the same magnification. Hybridization signals are in red. PC, perichondrium. (G-G1) Histology of the humerus from an E18.5 *Ihh$^{-/-}$* embryo. Asterisk in G indicates areas of vascularization. (G1) Area in yellow box (in G) is shown at a higher magnification in G1. Green lines indicate the outer (2) and inner (1) regions of the perichondrium; red and yellow arrows indicate cuboidal and elongated cells, respectively. (H-J1) In situ hybridization using ^{35}S-labeled riboprobes against *Runx2* (H,H1), *Osx* (I,I1) and *Ap* (J,J1) on sections adjacent to that in G. (H1-J1) Areas similar to that in G1, marked by yellow boxes in H-J, are shown at the same magnification as in G1. Hybridization signals are in red. Green lines demarcate the outer and inner regions of the perichondrium.

at the humerus in the DKO embryo (Fig. 4, compare B3 with C3) prompted us to examine the fate of the perichondrial mesenchymal cells at the diaphysis of the femur. Interestingly, at E18.5 in areas of the femur where no overt ossification had occurred, mesenchymal cells around the diaphysis (red asterisks, Fig. 7A,B) accumulated under the perichondrium ('PC', Fig. 7B), forming an asymmetrical 'mesenchymal collar'. Remarkably, the mesenchymal cells appeared to have migrated through the late hypertrophic chondrocytes splitting the hypertrophic zone ('H', Fig. 7A,C). Moreover, the mesenchymal cells embedded between the hypertrophic zones appeared to have died, resulting in an empty canal (green asterisk, Fig. 7C). The cell death correlated with the paucity of cartilage vascularization, which was reduced to small areas of the hypertrophic cartilage (Fig. 7D). More importantly, the viable mesenchymal cells beneath the perichondrium expressed markers of the osteoblast lineage, including *Ap*, *Osx* (Fig. 7B1-B2, respectively) and *Runx2* (data not shown), none of which was detected in the perichondrium ('PC'). The expression of these markers was not associated with hypertrophic chondrocytes as the cells did not express *Col10a1* (Fig. 7B3). Thus, in the DKO embryo, perichondrial mesenchymal cells accumulated around the diaphysis of the femur developed along the osteoblast lineage.

We next examined whether the perichondrial mesenchymal cells adopted a similar fate in the absence of canonical Wnt signaling. Similar to the DKO embryo, embryos with β-catenin selectively deleted in the skeleton (*Dermo1-Cre;* β-catenin$^{c/c}$) that we previously generated (Hu et al., 2005) also accumulated cells beneath the perichondrium at the diaphysis (Fig. 7E). There, as in the DKO embryo, orthotopic osteoblast development was also arrested prior to *Osx* activation (Hu et al., 2005). However, distinct from the DKO embryo, the *Dermo1-Cre;* β-catenin$^{c/c}$ embryo did not form ectopic bone at the diaphysis of the skeletal elements, despite advanced vascularization of the cartilage at E18.5 (Hu et al., 2005). Instead, cells accumulated beneath the perichondrium ('PC') exhibited the morphology of chondrocytes (red asterisks, Fig. 7E,F). Accordingly, the majority of the cells expressed high-levels of type II collagen (Col2a1) (Fig. 7F1) and the cells closer to the marrow cavity activated *Col10a1* expression (Fig. 7F2). Thus, in the absence of β-catenin, the perichondrial mesenchymal cells failed to form osteoblasts but instead developed into chondrocytes.

Finally, we examined the fate of the perichondrial cells in the E18.5 *Ihh$^{-/-}$* embryo. As noted earlier (Fig. 2), the perichondrium in the *Ihh$^{-/-}$* embryo was generally hypoplastic but slightly thickened at the diaphysis of the humerus (boxed region, Fig. 7G), where rudimentary vascularization occurred (asterisk, Fig. 7G). Moreover, the perichondrial cells within

this region underwent morphological differentiation (Fig. 7G1), as indicated by the cuboidal cells (red arrows) within the inner region (‘1’) versus the elongated cells (yellow arrows) at the outer region (‘2’). Importantly, the inner cells expressed *Runx2*, *Osx* and *Ap* (Fig. 7H1-J1, respectively) but not *Col10a1* (data not shown). Thus, in the *Ihh*$^{-/-}$ embryo, rudimentary vascularization correlated with early stages of osteoblastogenesis from the perichondrium.

Discussion

We have identified Gli3 as a key effector for Ihh signaling in the developing endochondral skeleton (Fig. 8A). Removal of Gli3 bypassed the requirement for Ihh in the proper proliferation and maturation of chondrocytes, indicating that Ihh normally regulates the progression of the cell cycle as well as expression of Pthlh by antagonizing the repressor activity of Gli3 (Gli3^{R}). The delay in chondrocyte maturation in the DKO embryo represents an ‘overcorrection’ phenotype and may reflect residual Gli3^{R} activities that escape Ihh antagonism in a normal embryo. However, orthotopic osteoblast differentiation, as well as vascularization of the hypertrophic cartilage, was only partially rescued in the DKO embryo. Thus, an additional effector(s), most probably one or more of the activator forms of the Gli molecules (Gli^{A}), is required for mediating the role of Ihh signaling in later development of osteoblasts and in specific aspects of cartilage vascularization.

The identity of Gli^{A} is presently unknown. Although Gli2^{A} has been shown to possess activator activities necessary for Shh signaling in both the central nervous system (Ding et al., 1998; Komori et al., 1997; Matise et al., 1998; Sasaki et al., 1999) and the developing hair follicle (Mill et al., 2003), Gli2$^{-/-}$ embryos exhibited only quantitative defects in bone formation (Miao et al., 2004). Thus, multiple Gli activators may function in combination to control progression of osteogenesis.

Notably, despite the rescue of cartilage proliferation and maturation, the limb skeletal elements of the DKO embryos remained considerably shorter than their wild-type counterparts. This finding underscores the important contribution of a normal bone collar (which failed to develop in the DKO embryo) to the overall linear growth of skeletal elements. Similarly, our previous studies showed that the Col2-Cre; Smo$^{n/c}$ mice, which had a similar proliferation defect as the Ihh$^{-/-}$ mutant but maintained a largely normal bone collar, exhibited a much milder growth defect than the Ihh$^{-/-}$ embryo (Long et al., 2001). Thus, development of the bone collar, together with growth of the cartilage, contributes to the linear length of a long bone.

The recovery of a low level of Ptch1 in the DKO embryo is consistent with a dual mechanism by which Ihh controls Ptch1 transcription: whereas a low level expression can be achieved by derepression of Gli3^{R}, the full activation of Ptch1 expression may require the activator forms of Gli molecules in response to robust Ihh signaling. Ptch1 was recently shown to be a direct transcription target of Gli proteins (Agren et al., 2004).

Despite the defect in cartilage vascularization in the DKO embryo, perichondrial mesenchymal cells independently invaded the hypertrophic cartilage. Thus, invasion of the mesenchymal cells can be uncoupled from cartilage vascularization. The molecular basis underlying the mesenchymal invasion is presently unknown but appears to be distinct from that for the blood vessel invasion, as *Mmp9* (Vu et al., 1998) was not expressed by the invading mesenchyme (data not shown).

Ihh signals via distinct transcriptional effectors at different stages of osteoblast development (Fig. 8B). Initially, Ihh activates expression of Runx2 and low levels of Col1a1 by counteracting the repressor function of Gli3 (Gli3^{R}) (‘1’). Further progression of the lineage, however, requires additional Ihh signaling, most probably transcriptional activation via Gli^{A} (‘2’). Previously, we showed that Ihh signaling activated canonical Wnt signaling which was in turn required for the activation of Osx expression (Hu et al., 2005). Thus, Gli^{A} is likely required to activate the canonical Wnt signaling, which

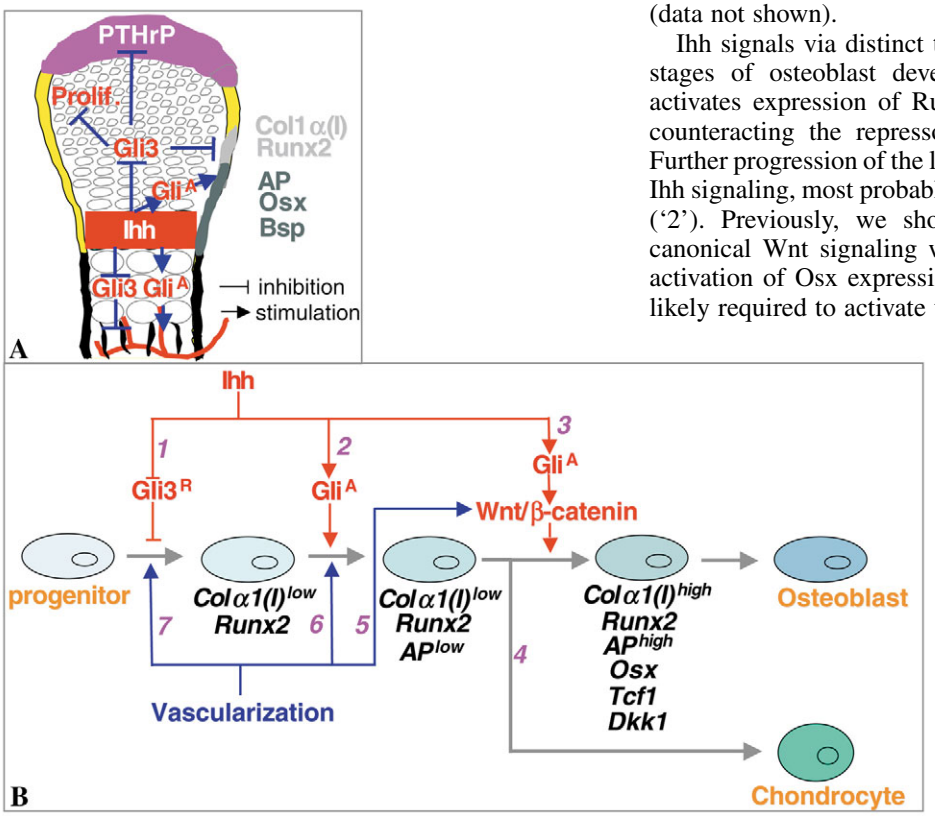

Fig. 8. Gli3 mediates multiple but not all aspects of Ihh signaling in the endochondral skeleton. (A) A summary of the roles of Gli3 and other effectors in mediating Ihh activity. Gli^{A}, activated form of Gli molecules. (B) A model for Ihh-versus vascularization-dependent osteoblast development. See text for details.

remained silent in the DKO embryo (‘3’). Alternatively, defective Wnt signaling could be secondary to earlier defects in the osteoblast lineage (e.g. absence of Ap^{low}-positive cells) in the DKO embryo.

The perichondrial mesenchymal cells are bi-potential for either osteoblasts or chondrocytes (Fig. 8B, ‘4’). In embryos of either *Dermo1Cre;* β-catenin$^{c/c}$ or DKO, the cells accumulated beneath the perichondrium at the diaphysis, forming a characteristic ‘wedge-shape’ mesenchyme. In the absence of β-catenin, the cells failed to express *Osx* and subsequently developed into chondrocytes, in a manner similar to that in the *Osx*$^{-/-}$ embryo (Nakashima et al., 2002). In the DKO embryo, *Osx* expression was activated in these cells, presumably by a vasculature-derived signal, and osteogenesis ensued. Thus, Osx appears to function as a molecular switch between the osteoblast and chondrocyte fates.

Chondrogenesis is unlikely a mere default fate for the perichondrial progenitors, as no chondrogenesis was observed in the perichondrium of the *Ihh*$^{-/-}$ embryo even though osteogenesis was impaired. Here, the perichondrium was generally hypoplastic, and no ‘wedge-shape’ mesenchyme was present at the diaphysis. In agreement with the absence of *Runx2* expression in the perichondrial cells prior to vascularization, the perichondrium phenotype here is similar to that in the *Runx2*$^{-/-}$ embryo (Komori et al., 1997; Otto et al., 1997), implicating Runx2 in the proper growth of the perichondrium. Similarly, in the *Runx2*$^{-/-}$ embryo, the perichondrial cells failed to undergo chondrogenesis, despite the defect in osteoblast development. These findings could indicate that Runx2 activity is required for the perichondrial cells to achieve their capacity for chondrocyte differentiation. Alternatively, the failure in chondrogenesis could be secondary to the perichondrium hypoplasia associated with Runx2 deficiency. Regardless of the mechanism, the absence of chondrogenesis in the *Ihh*$^{-/-}$ perichondrium seemed to be at odds with our previous finding that *Smo*$^{-/-}$ perichondrial cells (nonresponsive to Ihh) developed into chondrocytes (Long et al., 2004). However, the difference could be because the Ihh-nonresponsive cells in the previous study resided among wild-type cells in which Ihh signaling occurred. It is possible that secondary factors from the normal neighboring cells steered the Ihh-nonresponsive cells towards chondrogenesis.

Our results also indicate an osteogenic role for the vasculature (Fig. 8B). In this model, a signal from the vasculature could promote bone formation from *Col1a1*^{low}- and *Runx2*-postive cells (the ‘stalled’ cells in the DKO embryo) by activating *Ap* expression (‘6’) and the canonical Wnt/β-catenin pathway (‘5’). Moreover, a vascularization-dependent signal could initiate osteogenesis independent of Ihh signaling (as in the *Ihh*$^{-/-}$ embryo) (‘7’). It should be noted that we could not discern at present which mechanism contributed to the ‘ectopic’ bone in the DKO embryo. In addition, it is presently unknown whether mature osteoblasts can eventually develop in the *Ihh*$^{-/-}$ embryo as neonatal lethality of the mutant precludes analyses at later stages. However, a recent study reported that an *Ihh*$^{-/-}$ cartilage element, when implanted into the kidney capsule, became vascularized and developed bone, apparently without activating hedgehog signaling (Colnot et al., 2005). The nature of the vascularization-dependent signal is presently unknown but previous studies have implicated signals for the endothelium in development of the liver (Matsumoto et al., 2001) and the pancreas (Lammert et al., 2001). A definitive link between bone formation and endothelial signaling, however, awaits further studies.

The concept that vascularization functions as an osteogenic signal independent of Ihh has interesting implications. It follows that normally two distinct processes (Ihh dependent versus vascularization dependent) contribute to bone formation in the endochondral skeleton. Disruption of both in the *Ihh*$^{-/-}$ embryo resulted in a complete loss of bone. This notion could also explain the relatively normal intramembranous bones in the skull of the *Ihh*$^{-/-}$ embryo. As the skull bones are evolved earlier, does vascularization represent a more primitive and universal mechanism for bone formation, whereas Ihh dependence could be a recent invention to accommodate bone formation from a cartilage template?

We thank Dr Chin Chang (Vanderbilt University) for kindly providing the Gli3 antibody. We thank Drs Raphael Kopan and David Ornitz (Washington University Medical School) for critical reading of the manuscript. This work was supported by a NIH grant DK065789 (F.L.) and a NIH postdoctoral training grant 5T32AR07033 (M.J.H.).

References

Agren, M., Kogerman, P., Kleman, M. I., Wessling, M. and Toftgard, R. (2004). Expression of the PTCH1 tumor suppressor gene is regulated by alternative promoters and a single functional Gli-binding site. *Gene* **330**, 101-114.

Bai, C. B., Auerbach, W., Lee, J. S., Stephen, D. and Joyner, A. L. (2002). Gli2, but not Gli1, is required for initial Shh signaling and ectopic activation of the Shh pathway. *Development* **129**, 4753-4761.

Bai, C. B., Stephen, D. and Joyner, A. L. (2004). All mouse ventral spinal cord patterning by hedgehog is gli dependent and involves an activator function of gli3. *Dev. Cell* **6**, 103-115.

Buscher, D., Grotewold, L. and Ruther, U. (1998). The XtJ allele generates a Gli3 fusion transcript. *Mamm. Genome* **9**, 676-678.

Buttitta, L., Mo, R., Hui, C. C. and Fan, C. M. (2003). Interplays of Gli2 and Gli3 and their requirement in mediating Shh-dependent sclerotome induction. *Development* **130**, 6233-6243.

Chamorro, M. N., Schwartz, D. R., Vonica, A., Brivanlou, A. H., Cho, K. R. and Varmus, H. E. (2005). FGF-20 and DKK1 are transcriptional targets of beta-catenin and FGF-20 is implicated in cancer and development. *EMBO J.* **24**, 73-84.

Colnot, C., de la Fuente, L., Huang, S., Hu, D., Lu, C., St-Jacques, B. and Helms, J. A. (2005). Indian hedgehog synchronizes skeletal angiogenesis and perichondrial maturation with cartilage development. *Development* **132**, 1057-1067.

Ding, Q., Motoyama, J., Gasca, S., Mo, R., Sasaki, H., Rossant, J. and Hui, C. C. (1998). Diminished Sonic hedgehog signaling and lack of floor plate differentiation in Gli2 mutant mice. *Development* **125**, 2533-2543.

Gonzalez-Sancho, J. M., Aguilera, O., Garcia, J. M., Pendas-Franco, N., Pena, C., Cal, S., Garcia de Herreros, A., Bonilla, F. and Munoz, A. (2005). The Wnt antagonist DICKKOPF-1 gene is a downstream target of beta-catenin/TCF and is downregulated in human colon cancer. *Oncogene* **24**, 1098-1103.

Hu, H., Hilton, M. J., Tu, X., Yu, K., Ornitz, D. M. and Long, F. (2005). Sequential roles of Hedgehog and Wnt signaling in osteoblast development. *Development* **132**, 49-60.

Karp, S. J., Schipani, E., St-Jacques, B., Hunzelman, J., Kronenberg, H. and McMahon, A. P. (2000). Indian hedgehog coordinates endochondral bone growth and morphogenesis via parathyroid hormone related-protein-dependent and -independent pathways. *Development* **127**, 543-548.

Komori, T., Yagi, H., Nomura, S., Yamaguchi, A., Sasaki, K., Deguchi, K., Shimizu, Y., Bronson, R. T., Gao, Y. H., Inada, M. et al. (1997). Targeted disruption of Cbfa1 results in a complete lack of bone formation owing to maturational arrest of osteoblasts. *Cell* **89**, 755-764.

Lammert, E., Cleaver, O. and Melton, D. (2001). Induction of pancreatic differentiation by signals from blood vessels. *Science* **294**, 564-567.

Lanske, B., Karaplis, A. C., Lee, K., Luz, A., Vortkamp, A., Pirro, A., Karperien, M., Defize, L. H., Ho, C., Mulligan, R. C. et al. (1996).

PTH/PTHrP receptor in early development and Indian hedgehog-regulated bone growth. *Science* **273**, 663-666.

Li, Y., Zhang, H., Choi, S. C., Litingtung, Y. and Chiang, C. (2004). Sonic hedgehog signaling regulates Gli3 processing, mesenchymal proliferation, and differentiation during mouse lung organogenesis. *Dev. Biol.* **270**, 214-231.

Litingtung, Y. and Chiang, C. (2000). Specification of ventral neuron types is mediated by an antagonistic interaction between Shh and Gli3. *Nat. Neurosci.* **3**, 979-985.

Litingtung, Y., Dahn, R. D., Li, Y., Fallon, J. F. and Chiang, C. (2002). Shh and Gli3 are dispensable for limb skeleton formation but regulate digit number and identity. *Nature* **418**, 979-983.

Long, F., Zhang, X. M., Karp, S., Yang, Y. and McMahon, A. P. (2001). Genetic manipulation of hedgehog signaling in the endochondral skeleton reveals a direct role in the regulation of chondrocyte proliferation. *Development* **128**, 5099-5108.

Long, F., Chung, U. I., Ohba, S., McMahon, J., Kronenberg, H. M. and McMahon, A. P. (2004). Ihh signaling is directly required for the osteoblast lineage in the endochondral skeleton. *Development* **131**, 1309-1318.

Matise, M. P., Epstein, D. J., Park, H. L., Platt, K. A. and Joyner, A. L. (1998). Gli2 is required for induction of floor plate and adjacent cells, but not most ventral neurons in the mouse central nervous system. *Development* **125**, 2759-2770.

Matsumoto, K., Yoshitomi, H., Rossant, J. and Zaret, K. S. (2001). Liver organogenesis promoted by endothelial cells prior to vascular function. *Science* **294**, 559-563.

Maynard, T. M., Jain, M. D., Balmer, C. W. and LaMantia, A. S. (2002). High-resolution mapping of the Gli3 mutation extra-toes reveals a 51.5-kb deletion. *Mamm. Genome* **13**, 58-61.

McLeod, M. J. (1980). Differential staining of cartilage and bone in whole mouse fetuses by alcian blue and alizarin red S. *Teratology* **22**, 299-301.

Miao, D., Liu, H., Plut, P., Niu, M., Huo, R., Goltzman, D. and Henderson, J. E. (2004). Impaired endochondral bone development and osteopenia in Gli2-deficient mice. *Exp. Cell. Res.* **294**, 210-222.

Mill, P., Mo, R., Fu, H., Grachtchouk, M., Kim, P. C., Dlugosz, A. A. and Hui, C. C. (2003). Sonic hedgehog-dependent activation of Gli2 is essential for embryonic hair follicle development. *Genes Dev.* **17**, 282-294.

Mo, R., Freer, A. M., Zinyk, D. L., Crackower, M. A., Michaud, J., Heng, H. H., Chik, K. W., Shi, X. M., Tsui, L. C., Cheng, S. H. et al. (1997). Specific and redundant functions of Gli2 and Gli3 zinc finger genes in skeletal patterning and development. *Development* **124**, 113-123.

Motoyama, J., Liu, J., Mo, R., Ding, Q., Post, M. and Hui, C. C. (1998). Essential function of Gli2 and Gli3 in the formation of lung, trachea and oesophagus. *Nat. Genet.* **20**, 54-57.

Nakashima, K., Zhou, X., Kunkel, G., Zhang, Z., Deng, J. M., Behringer, R. R. and de Crombrugghe, B. (2002). The novel zinc finger-containing transcription factor osterix is required for osteoblast differentiation and bone formation. *Cell* **108**, 17-29.

Niida, A., Hiroko, T., Kasai, M., Furukawa, Y., Nakamura, Y., Suzuki, Y., Sugano, S. and Akiyama, T. (2004). DKK1, a negative regulator of Wnt signaling, is a target of the beta-catenin/TCF pathway. *Oncogene* **23**, 8520-8526.

Otto, F., Thornell, A. P., Crompton, T., Denzel, A., Gilmour, K. C., Rosewell, I. R., Stamp, G. W., Beddington, R. S., Mundlos, S., Olsen, B. R. et al. (1997). Cbfa1, a candidate gene for cleidocranial dysplasia syndrome, is essential for osteoblast differentiation and bone development. *Cell* **89**, 765-771.

Park, H. L., Bai, C., Platt, K. A., Matise, M. P., Beeghly, A., Hui, C. C., Nakashima, M. and Joyner, A. L. (2000). Mouse Gli1 mutants are viable but have defects in SHH signaling in combination with a Gli2 mutation. *Development* **127**, 1593-1605.

Roose, J., Huls, G., van Beest, M., Moerer, P., van der Horn, K., Goldschmeding, R., Logtenberg, T. and Clevers, H. (1999). Synergy between tumor suppressor APC and the beta-catenin-Tcf4 target Tcf1. *Science* **285**, 1923-1926.

Sasaki, H., Nishizaki, Y., Hui, C., Nakafuku, M. and Kondoh, H. (1999). Regulation of Gli2 and Gli3 activities by an amino-terminal repression domain: implication of Gli2 and Gli3 as primary mediators of Shh signaling. *Development* **126**, 3915-3924.

St-Jacques, B., Hammerschmidt, M. and McMahon, A. P. (1999). Indian hedgehog signaling regulates proliferation and differentiation of chondrocytes and is essential for bone formation. *Genes Dev.* **13**, 2072-2086.

Vortkamp, A., Lee, K., Lanske, B., Segre, G. V., Kronenberg, H. M. and Tabin, C. J. (1996). Regulation of rate of cartilage differentiation by Indian hedgehog and PTH-related protein. *Science* **273**, 613-622.

Vu, T. H., Shipley, J. M., Bergers, G., Berger, J. E., Helms, J. A., Hanahan, D., Shapiro, S. D., Senior, R. M. and Werb, Z. (1998). MMP-9/gelatinase B is a key regulator of growth plate angiogenesis and apoptosis of hypertrophic chondrocytes. *Cell* **93**, 411-422.